Application of Carbons Produced from Rice Husk in the Process of Capacitive Deionization

V. Pavlenko[1,2]* and Zh. Supiyeva[1,2]

[1]Institute of Combustion Problems, 172 Bogenbay Batyr str., Almaty, Kazakhstan
[2]al-Farabi Kazakh National University, 71 al-Farabi ave., Almaty, Kazakhstan

Article info	Abstract
	Nanoporous carbon materials are well recognized as the main components of electrodes in capacitive deionization. Herein, the activated carbons were produced based on rice husk which is an abundant waste material in southern regions of Kazakhstan. The resulting carbons were characterized electrochemically by comparing their performance with well-known brands of commercial porous carbons (i.e. Norit DLC Super 30, Kuraray YP 50F). The features of carbon/carbon electrochemical cells were analyzed using the means of galvanostatic cycling with potential limitation and cyclic voltammetry. Whilst the surface morphology and elemental composition of carbons were observed using scanning electron microscopy combined with energy dispersive X-ray spectroscopy. Using the method of low-temperature nitrogen adsorption it has been established that the specific surface of home-made carbon produced based on rice husk is equal to 2290 m^2g^{-1}. The salt adsorption analysis has been performed using different concentrations of inlet solutions of sodium chloride. Our study has shown that the manufacturing and application of activated carbons based on rice husk can be highly efficient because the resulting electrode materials exhibit a high electrosorption capacity of 20.02 mg g^{-1}, which exceeds similar values obtained in the case of application of commercial porous carbons.

1. Introduction

Capacitive deionization (CDI) is a modern method of water desalination which has been recognized to have high economic feasibility [1]. Structurally it includes a pumping system of an aqueous solution through an electrochemical cell consisting of two porous electrodes having a highly developed surface, between which a certain potential difference is set [1–3]. When an electric current is applied to the electrodes, a potential difference arises, and an electric double layer (EDL) is formed on the surface of the polarized electrodes. The formation of an electric double layer is accompanied, respectively, by the adsorption of anions on the positive electrode and cations on the negative electrode.

*Corresponding author.
E-mail: pavlenko-almaty@mail.ru

This charging-discharging process of the electric double layer is similar to that for supercapacitors [4]. Under the influence of an electric field, anions are adsorbed on the positive electrode, and cations on the negative electrode, and thus the electric double-layer is charged. As a result, deionization (desalination) of the aqueous solution takes place. After the electrodes are saturated with adsorbed ions, a significantly smaller water flow is supplied to the electrochemical cell and at the same time the voltage in the external circuit is turned off or a polarity reversal is organized. This leads to the desorption of ions from the electrodes and their concentration in the second stream [5–6].

In [7–8], carbon electrodes were synthesized using the PVA binder through a cross-linking method. It was shown that the application of carbon electrodes having hydrophilic properties allowing

to increase in the wetted surface area, enhances the efficiency of CDI process. All carbon electrodes exhibited their capability to slightly adsorb ions on the electrode surface. The percentage of salt removal (0.1 mol L^{-1} NaCl, MgCl and KCl) was examined in [8]. When the potentials of 1.0, 2.0, and 3.0 V were applied to the CDI cell, the result showed that a 0.1 mol L^{-1} KCl solution had a greater percentage of salt removal than the solutions of NaCl and MgCl having the same concentration of ions dissolved. The percentage of salt removal from KCl was achieved at 55% for 3.0 V, while for NaCl and MgCl 20 and 30% were obtained, respectively [7–8].

A novel liquid binder used in the preparation of electrodes from activated carbon for application in CDI process was synthesized on a basis of acrylic acid and azodiisobutyronitrile [9]. As a result, its wettability was significantly improved, and the specific capacitance was increased by a factor of 8. The optimization showed that electrodes with a mass fraction of activated carbon of 35 wt% had the best CDI performance.

Up-to-date progress on the fabrication of electrode materials applicable in CDI process was reviewed in [10]. Herein, the fundamental principal (e.g. EDL theory and adsorption isotherms) as well as process factors (e.g. pore distribution, potential, salt type and concentration) of CDI performance were discussed. It was then followed by in-depth discussion and comparison on properties and fabrication technique of different electrodes, including carbon aerogel, activated carbon, carbon nanotubes, graphene and ordered mesoporous carbon. Novel nanomaterials such as graphene and CNTs are attracting increased attention in this area due to their extremely high specific surface area and electrical conductivity. It is noteworthy that polyaniline (PANI) as conductive polymer has a great potential for application in the CDI processes as electrode-enhancing materials. It was envisaged that large scale PANI-assisted CDI electrode fabrication can be plausible due to its low cost, mechanical flexibility and good electrical properties [10].

Carbon electrodes for the desalination system have been successfully synthesized with and / or without modified activated carbon by chemical activation using HNO$_3$. The results showed that the percentage of salt removal using the carbon electrodes with a modified activated carbon is higher than the carbon electrodes without modification of activated carbon, whilst the reduction level is equal to 55.7 and 24.8%, respectively [11].

Application in the CDI process of carbide-derived carbon (CDC) representing porous material with well-defined and tunable pore sizes in the sub-nanometer range was reported in [12]. Comparison of the electrode composites based on CDC with composites based on activated carbon showed that the former has a significantly higher salt adsorption capacity in the relevant cell voltage window of 1.2–1.4 V [12]. The measured adsorption capacity for four materials tested negatively correlates with known indicators for the pore structure of carbon powders, such as the total pore volume and BET area. But at the same time, it positively correlates with pore volumes with sizes <1 nm, which indicates the relevance of these subnanometer pores for ion adsorption. The charge efficiency, which is the ratio of the equilibrium salt adsorption to charge, does not depend much on the type of material, which indicates that materials that have been identified for high charge storage capacity can also be very suitable for CDI. For CDI, the most promising materials for electrodes are those which have a high specific surface area, a large number of subnanometric pores, good electrical conductivity and low cost [13–19]. Due to these properties, nanoporous carbons have attracted the attention of researchers around the world [20–22].

Porous carbon materials utilized in this study include two commercially available activated carbon powders, particularly the Norit DLC Super 30 (Calgon Carbon) and Kuraray YP 50F (Cabot). The home-made activated carbons were synthesized from rice husk (RH) through its carbonization and subsequent chemical activation processes. The objective of this work was to determine the most optimal conditions of the desalination process while electrosorbing in porous electrodes. For this reason, the various electrode materials and experimental parameters were investigated.

2. Experimental

2.1. Preparation of electrode materials

The rice husk (RH) was derived from local farms of Almaty region (Kazakhstan) and subjected for cleaning and drying to constant mass followed by carbonization at 500 °C ±10 °C under nitrogen atmosphere for 1 h. Chemical activation was carried out at 800 °C ±10 °C under nitrogen atmosphere for 1 h. Potassium hydroxide was used as an activating agent, while the mass ratio of precursor to KOH equal to 1:4 was applied.

The resulting samples were cleaned by deionized water until pH value ~7 and dried at 100 °C for 24 h. RH based activated carbon prepared this way was further implemented as electrode material in CDI using the technique described below.

Electrodes were prepared from three carbon materials: Norit DLC Super 30 (DLC Super 30), Kuraray YP 50F (KYP 50F) and rice husk based activated carbon (RH-AC). For each electrode preparation, 85 wt% activated carbon (AC) was mixed with 5 wt% carbon black (C65) and 10 wt% polytetrafluoroethene (PTFE). Carbon powders were blended with the binder in isopropanol used as the solvent. Next, they were rolled using a calendaring machine until achieving the demanded thickness of 500 μm. Materials were then dried under vacuum at 120 °C for 12 h.

2.2. Characterization

In order to investigate the morphology of samples, the scanning electron microscopy (SEM) combined with energy dispersive X-ray Spectroscopy (EDS) was conducted using the S-3400N SEM (Hitache).

The porous texture of carbons was characterized by nitrogen adsorption/desorption at -196 °C using the ASAP 2020 (Micromeritics). Prior to the analyses, the samples were degassed at 350 °C for 12 h under vacuum. The pore size distribution was determined based on the two-dimensional non-local density functional theory (2D-NLDFT) [22] model assuming an energetic heterogeneity of carbon pores. The average micropore size L_0 was determined from the Stoeckli equation [23].

All electrochemical experiments were carried out using a multi-channel potentiostat/galvanostat VMP3 (Biologic) using chronoamperometry with charging voltage up to 1.2 V, cyclic voltammetry (CV) at different scan rates and galvanostatic cycling with potential limitation (GCPL) with a potential limit up to 1.2 V and a constant current of 200 mA g^{-1} methods.

The specific capacitance (C_{sp} in F g^{-1}) of samples can be calculated from the CV measurement according to Eq. (1) [18]:

$$C_{sp} = \frac{\int i\,dt}{m\Delta VS} \tag{1}$$

where i (A) is the current, s (V s^{-1}) is the scan rate, ΔV (V) is the voltage window, t (s) is the time and m (g) is the mass of the electrode.

2.3. CDI measurement

A CDI installation included influent and effluent reservoirs, peristaltic pump, conductivity meter (CPC-501), CDI module, pH meter (Elmeiron) and potentiostat-galvanostat. The relationship between conductivity and molar concentration was obtained according to the calibration curve. Ions were electrosorbed from the solution by applying the direct voltage of 1.2 V between pair of electrodes. Solutions of 5, 10, 50 and 100 mmol L^{-1} NaCl (Sigma Chempur) were prepared by measuring NaCl crystals on an analytical balance and diluting in a volumetric flask. The flow rate of the peristaltic pump was equal to 5 mL/min.

The equilibrium electrosorption capacity (S, mg g^{-1}) per mass of electrode was defined as following Eq. (2) [19]:

$$S = \frac{(C_0 - C_e)V}{M} \tag{2}$$

where C_0 and C_e represent initial and equilibrium concentrations of NaCl solution (mg L^{-1}), respectively, V is the volume of solution (L), and M is the mass of the electrodes (g).

3. Results and discussion

The microstructure and morphology of the ACs obtained on the basis of RH were investigated using the SEM analyses, while the micrographs are shown in Fig. 1a on which one can see that the sample of RH-AC is irregularly granular. SEM images represented in Fig. 1b,c,d demonstrate morphological features of the surface texture of RH-AC representing the AC obtained by carbonization and activation of RH. The sample is characterized by a porous structure with macropores of various diameters from 10 μm and below. The material of the home-made AC is represented by the existence of macroscopic ensembles of ultrafine particles with the size from 50 to 300 μm. It is noted that the surface morphology is loose, formed by a system of pores and channels formed by the nature to ensure plant life.

Application of potassium hydroxide for the chemical activation of preliminary carbonized RH resulted in the production of ACs with an outstanding porous structure, openwork surface and texture morphology, as can be seen from Fig. 1b,c,d. The general appearance of the material has common morphological features, such as the channel
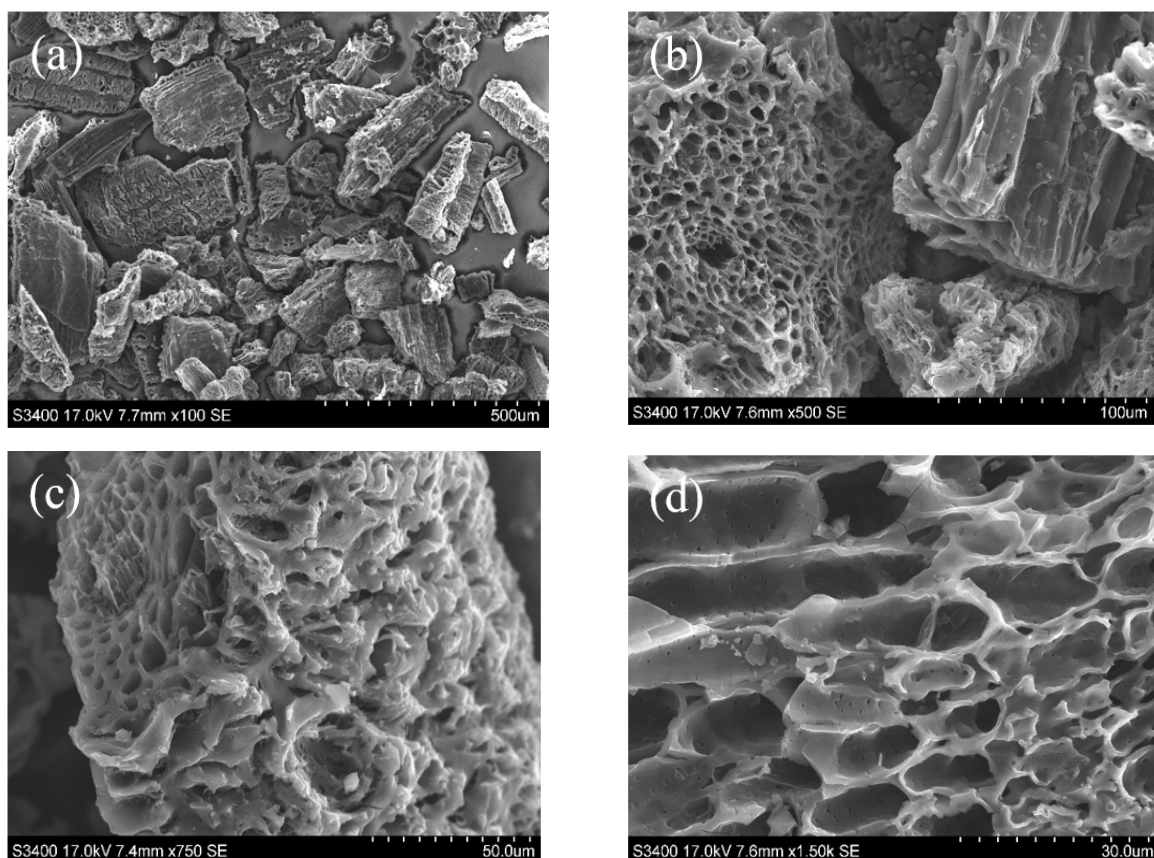
Fig. 1. SEM images of rice husk based AC at magnifications of (a) x100, (b) x500, (c) x750, and (d) x1500.

structure of macropores, which is a typical characteristic of carbonized and chemically activated plant materials. In turn, the presence of macropores on the surface of the obtained materials can serve as a necessary transport system due to which the electrolyte diffuses rapidly into the mesopores and further in micropores that making the main contribution to the formation of the specific surface area.

It is known that the physicochemical composition of the RH is characterized by the presence of a large amount of amorphous silicon oxide, the content of which in the original fibers varies at a level of 20 wt% [24]. Despite this, due to the preliminary leaching of carbonized RH by sodium hydroxide, a resulting content of SiO_2 or any other mineral component of resulting carbonaceous material becomes lower than the detecting limit of EDS apparatus (<0.5 wt%). Generally, as it can be seen from Fig. 2, elemental composition of RH-based AC is represented by carbon and oxygen which contents are approximately equal to 89 wt% and 10 wt%, respectively.

Isotherms of the low-temperature nitrogen adsorption-desorptionand details of pore size distribution are illustrated in Fig. 3a,b and summarized in Table. The isotherms of ACs shown in Fig. 3a

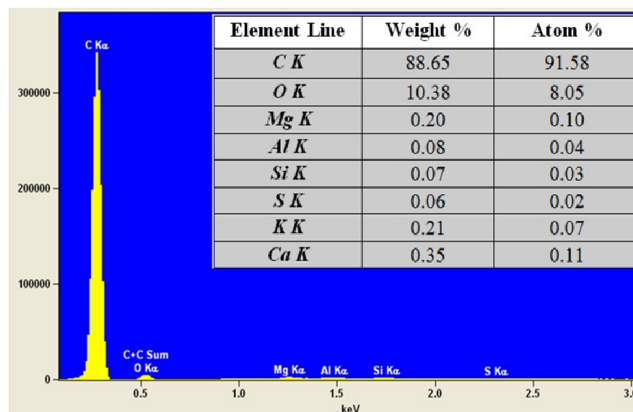| Element Line	Weight %	Atom %
C K	88.65	91.58
O K	10.38	8.05
Mg K	0.20	0.10
Al K	0.08	0.04
Si K	0.07	0.03
S K	0.06	0.02
K K	0.21	0.07
Ca K	0.35	0.11

Fig. 2. Energy-dispersive X-ray spectra of rice husk based AC (inlet – elemental analysis data).

correspond to Type I, which is typical for microporous materials (pore size d <2 nm). Meanwhile, at high relative pressure only minor hysteresis loops can be detected, which can indicate an existence of a small fraction of mesopores (pore size $2 \leq d \leq 50$ nm). Herein, the RH-AC possesses the highest nitrogen uptake, which suggests a highly developed porous structure. As is shown in Table, the specific surface area of RH-AC is 2290 m²/g. The aforementioned value is bigger than of KYP

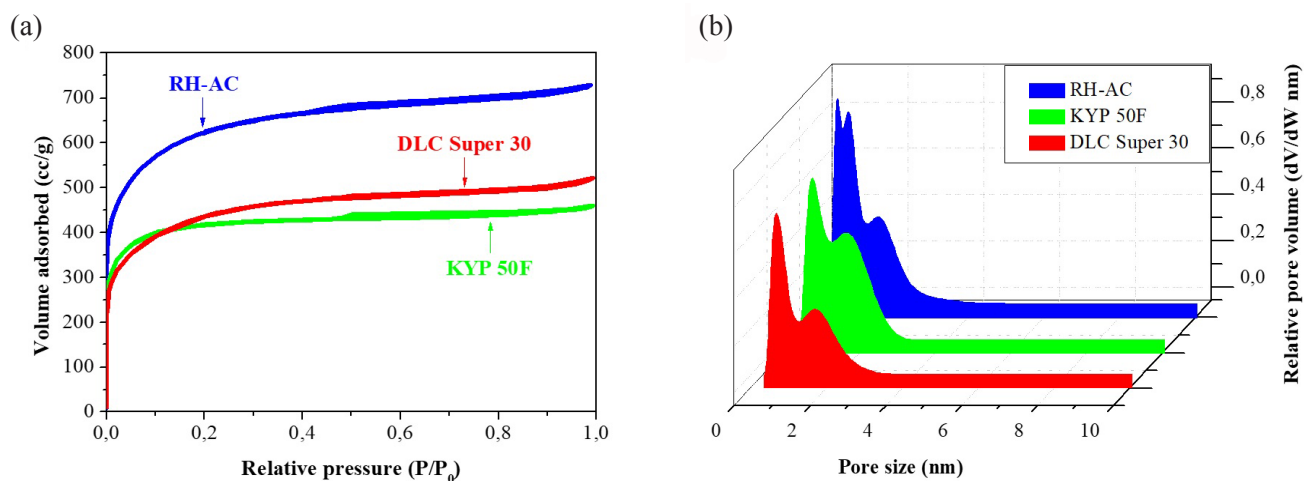Fig. 3. Parameters of porous texture: (a) Nitrogen adsorption/desorption isotherms realized at -196 °C, (b) pore size distribution.

Table
Porosity parameters of various electrodes

Sample	BET surface area [m²/g]	Cumulative surface area [m²/g]	V_{micro} < 2[nm] [cm³/g]	V_{meso} 2-50 [nm] [cm³/g]	Average micropores size (L_0) [nm]	Average mesopores size (L_0) [nm]
RH-AC	2290	1990	0.80	0.18	0.88	4.12
KYP 50F	1560	1401	0.60	0.05	0.87	5.25
DLC SUPER 30	1598	1332	0.57	0.17	0.92	3.15

50F, DLC SUPER 30 which are equal to 1560 m²/g and 1598 m²/g, respectively. On other hand, the pore size distribution represented in Fig. 3b indicates that RH-AC has a big fraction of ultra-micropores (<0.7 nm), which have a higher adsorption potential towards the small ions, i.e. Na⁺, Cl⁻ dissolved in water.

From the obtained voltammograms illustrated in Fig. 4a, it was observed that all three types of electrode materials exhibit the nearly rectangular shape of cyclic voltammetry curves CVs, indicating a capacitive behavior that mainly arises from the charge and discharge of the EDL [20]. The highest capacitive current was observed for 2E cells based on RH-AC, while the lowest one for YP50F. It is indicated, that capacitive current is higher for the materials with the higher specific surface area. Thereby, one can see a correlation between this current and the textural parameters, e.g. specific surface area of the materials. However, it should be noted that the trapping of ions is also influenced by the relative relationship between the size of pores and ions. Moreover, in the case of galvanostatic charging/discharging all three tested materials display a typical triangular shape (Fig. 5b). The cells assembled with RH-AC exhibits the highest capacitance which is equal to 94 F g⁻¹, but meanwhile, it has the lowest coloumbic efficiency and charge propagation properties. In turn, the DLC Super 30 and KYP 50F display moderate capacitance equal to 85 F g⁻¹ and 81 F g⁻¹, respectively. The 2E cell based on DLC Super 30 exhibits the highest coloumbic efficiency of 98%.

An experimental installation for CDI of water solutions illustrated in Fig. 5 was used to investigate the electrosorption performance of different electrode materials based on DLC Super 30, KYP 50F and RH-AC. The CDI experiments were realized in NaCl solution which had an initial conductivity of 574 μS cm⁻¹. Figure 6a shows the variation of solution conductivity versus time. It can be seen that all the curves display a similar shape, and reach an electrosorption saturation after charging for about 30 min. Additionally, the lowest conductivity of outlet solution equal to 495 μS cm⁻¹ was obtained when the electrodes based on RH-AC were applied, whereas the similar values for KYP 50F and DLC Super 30 were equal to 511 μS cm⁻¹ and 505 μS cm⁻¹, respectively.
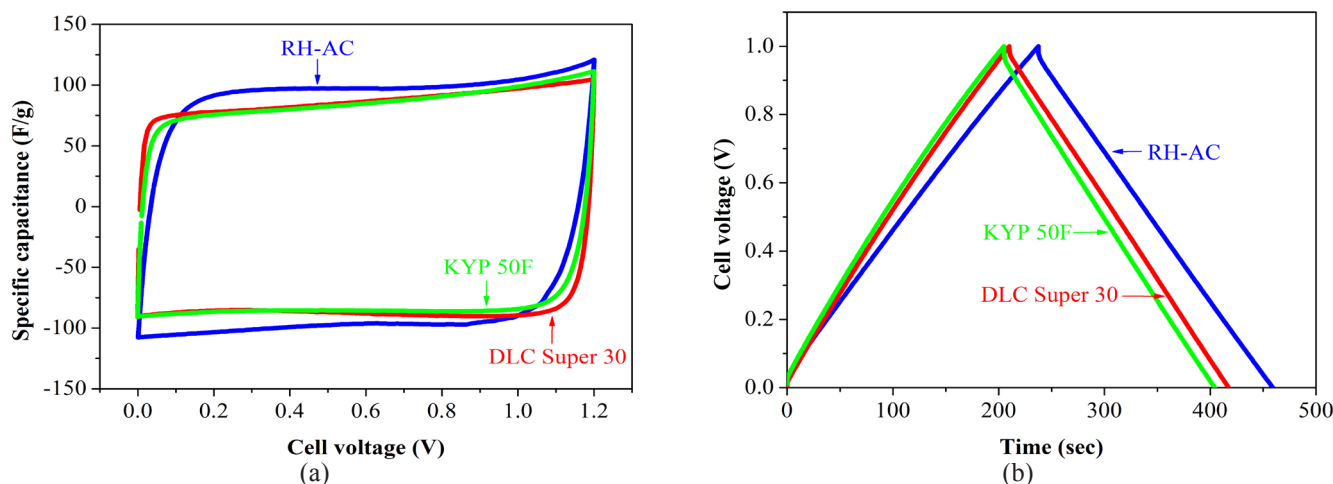
Fig. 4. (a) CV of 2E cells assembled in 100 mmol L^{-1} NaCl at 5 mV s^{-1}, (b) GCPL cuves at 200 mA g^{-1}.
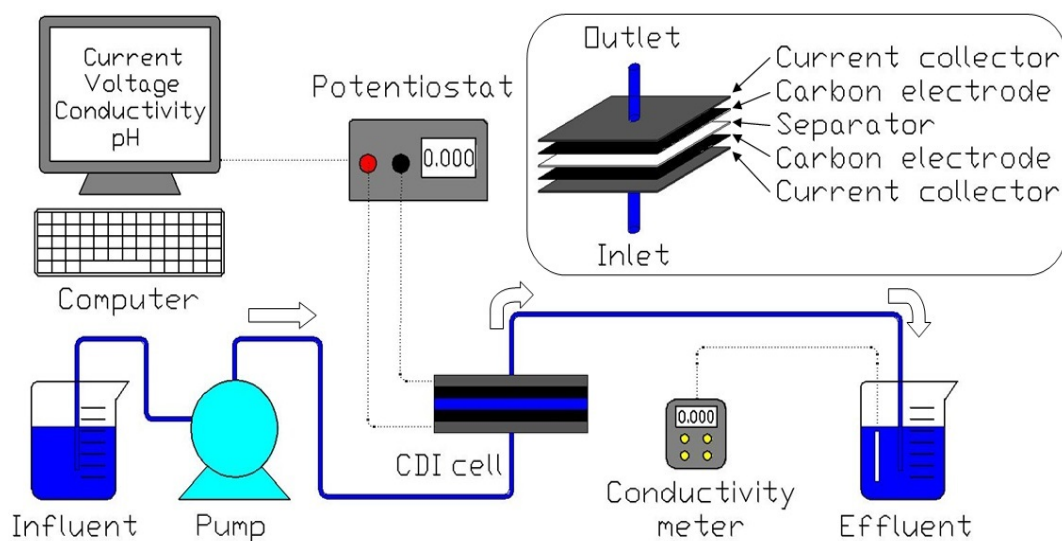

Fig. 5. Principle scheme used for capacitive deionization of brackish water solutions.

The kinetics of the desalination during the CDI process with different electrodes has been exemplified in Fig. 6b. Herein, one can see that the electrosorption capacities were raising along with the increase of time before they reached the aforementioned values. In turn, the Ragone plots illustrated in Fig. 6c were employed to measure the rate and electrosorption capacity of the as-prepared electrodes. It is noted that the curve corresponding to the electrodes based on RH-AC is located in the upper and righter region of Ragone plots, which means that they possess the largest electrosorption capacity and fastest electrosorption rate. In other words, since the RH-AC possesses higher values of specific surface area and specific capacitance than of KYP 50F and DLC Super 30, thereby the former provides more area to store ions in terms of formation of an electrical double layer.

In order to further explore the CDI performance of as-prepared electrodes, the CDI electrosorption experiments at different initial concentrations were realized. RH-AC electrode possesses an improved electrosorption capacity at all initial concentrations compared to KYP 50F and DLC Super 30 electrode composites (Fig. 6d). As can be seen from Fig. 6d, the salt retention capacity increases from 8.74 to 20.05 mg g^{-1} for RH-AC and from 6.97 to 15.84 mg g^{-1} for KYP 50F with increasing NaCl concentration from 5 to 100 mmol L^{-1}.

From the electrosorption experiments it has been revealed that among three different type of electrodes, the one which is based on RH-AC can adsorb the largest amount of ions from the aqueous solutions of NaCl. According to Eq. (2), the electrosorption capacities of electrodes based on RH-AC, KYP 50F and DLC Super 30 electrodes were equal to 8.74, 6.97 and 7.59 mg g^{-1}, respectively.

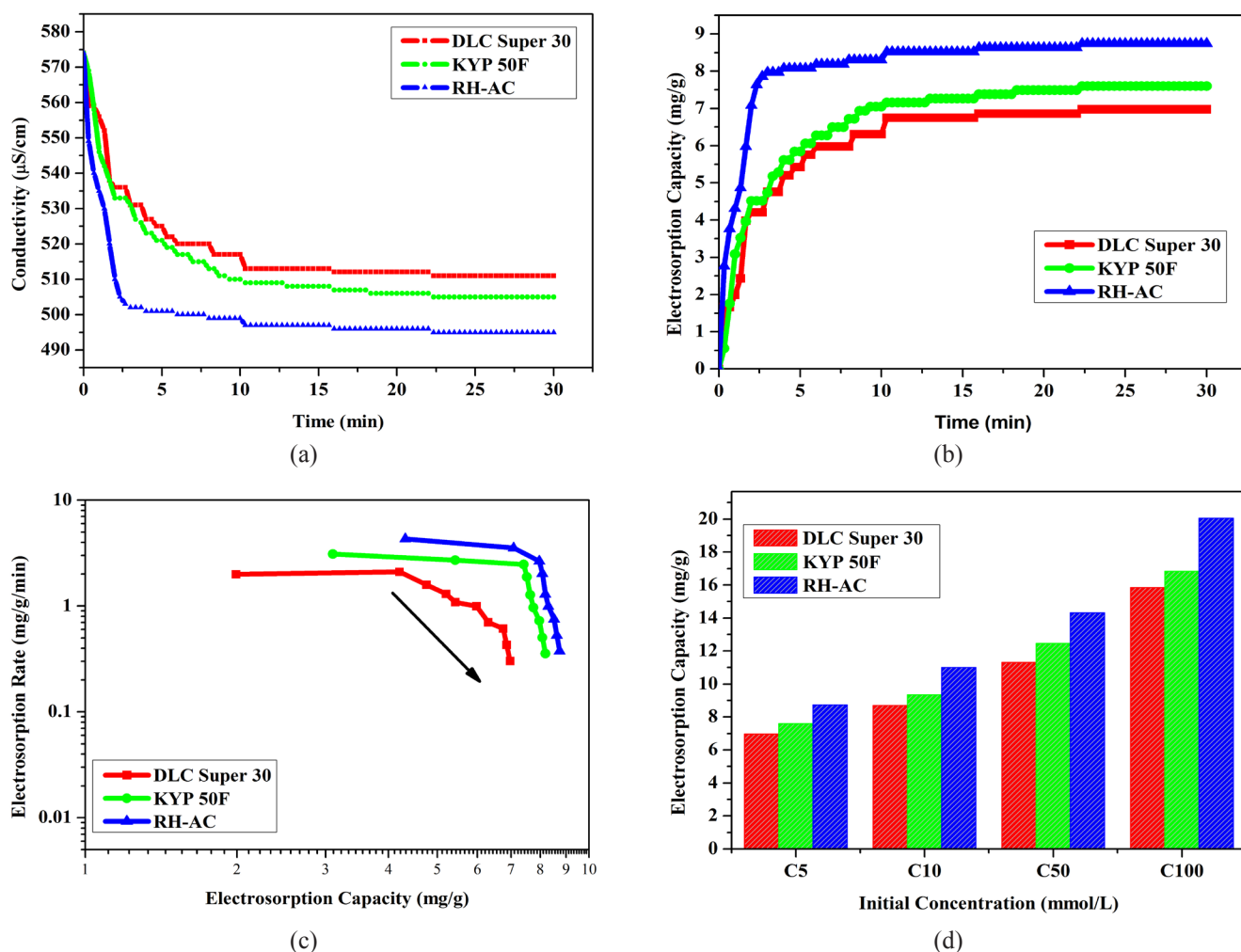Fig. 6. (a) CDI profiles of solution conductivity vs time, (b) electrosorption kinetics and (c) Ragone plots of DLC Super 30, KYP 50F and RH-AC electrodes in a 5 mmol L^{-1} NaCl solution; (d) electrosorption capacities in NaCl solution with different initial concentrations at 1.2 V.

Generally, the investigation of CDI electrosorption performance using the different ACs showed a common decrease in conductivity after the electrical voltage was applied. Wherein, the electrode composites based on RH-AC exhibits the electrosorption capacity of 20.05 mg g^{-1} in 100 mmol L^{-1} NaCl solution at 1.2 V, which is sufficiently higher than those of KYP 50F and DLC Super 30. Consequently, it has been established that an application of the carbonized and activated RH in producing electrode composites to be suitable for water desalination through the CDI technology.

4. Conclusions

It was shown that the CDI is a quick and efficient technology for the desalination of water with a low content of salt (up to 100 mmol L^{-1}). Moreover, within the scope of this study, we have investigated the CDI performances of different carbon materials including the home-made porous carbon produced on the basis of RH, as well as two brands of commercial ACs represented by DLC Super 30 and KYP 50F. The application of chronoamperometry allowed us to evaluate the high reversibility and cyclability of CDI process within the same configuration of electrochemical cells. It is shown that the enhanced efficiency of salt removal can be obtained when the increased concentrations of salt are implemented. Besides, it is claimed that microporous carbons presumably possess high adsorption potentials which are particularly effective for use in CDI processes, although a certain amount of mesopores in carbon electrodes can be attractive to enhance the diffusion kinetics.

Our study shows that the manufacturing of low-cost ACs based on RH can be highly effective for application as electrode composites. In particular, the resulting porous carbons can be implemented to store the an energy in electric double layer and

to serve as a useful material for salts adsorption. On other hand, the values of adsorption capacity and charge efficiency are in good agreement with previously published data, which confirms a high performance of the systems designed.

Acknowledgments

References

[1]. J.C. Farmer, D.V. Fix, G.V. Mack, R.W. Pekala, J.F. Poco, *J. Electrochem. Soc.* 143 (1996) 159–169. DOI: 10.1149/1.1836402

[2]. P. Xu, J.E. Drewes, D. Heil, G. Wang, *Water Res*. 42 (2008) 2605–2617. DOI: 10.1016/j.watres.2008.01.011

[3]. R. Zhao, P.M. Biesheuvel, H. Miedema, H. Bruning, *J. Phys. Chem. Lett.* 1 (2010) 205–210. DOI: 10.1021/jz900154h

[4]. E. Pamete Yambou, B. Gorska, V. Pavlenko, F. Béguin, *Electrochim. Acta* 350 (2020) 136416. DOI: 10.1016/j.electacta.2020.136416

[5]. Y.J. Kim, J.H. Choi, *Water Res.* 44 (2010) 990–996. DOI: 10.1016/j.watres.2009.10.017

[6]. Y. Gao, L.K. Pan, H.B. Li, Y.P. Zhang, Z.J. Zhang, Y.W. Chen, Z. Sun, *Thin Solid Films* 517 (2009) 1616–1619. DOI: 10.1016/j.tsf.2008.09.065

[7]. Endarko, N. Fadilah, D. Anggoro, *AIP Conference Proceedings* 1719 (2016) 030026. DOI: 10.1063/1.4943721

[8]. D. Anggoro, Endarko, *Advanced Materials Research Submitted* 1112 (2014) 271–274. DOI: 10.4028/www.scientific.net/AMR.1112.271

[9]. L. Chang, Y. Yu, X. Duan, W. Liu, *Sep. Sci. Technol.* 48 (2013) 359–365. DOI: 10.1080/01496395.2012.675000

[10]. B. Jia, W. Zhang, *Nanoscale Res. Lett.* 11 (2016) 64. DOI 10.1186/s11671-016-1284-1

[11]. D.A. Nisa, Endarko, *IOP Conf. Ser.: Mater. Sci. Eng.* 214 (2017) 012024. DOI: 10.1088/1757-899X/214/1/012024

[12]. S. Porada, L. Weinstein, R. Dash, A. van der Wal, M. Bryjak, Y. Gogotsi, P.M. Biesheuvel, *ACS Appl. Mater. Interfaces* 4 (2012) 1194−1199. DOI: 10.1021/am201683j

[13]. C. Feng, Y.-A. Chen, C.-P. Yu, *Chemosphere* 208 (2018) 285−293. DOI: 10.1016/j.chemosphere.2018.05.174

[14]. Y. Bouhadana, E. Avraham, M. Noked, M. Ben-Tzion, A. Soffer, D. Aurbach, *J. Phys. Chem. C* 115 (2011) 16567–16573. DOI: 10.1021/jp2047486

[15]. S.K. Sami, J.Y. Seo, S-E. Hyeon, Md. S.A. Shershah, P.-J. Yoo, C.-H. Chung, *RSC Adv.* 8 (2018) 4182–4190. DOI: 10.1039/C7RA12764B

[16]. S. Rezma, I.B. Assaker, Y. Litaiem, R. Chtourou, A. Hafiane, H. Deleuze, *Mater. Res. Bull.* 111 (2019) 222–229. DOI: 10.1016/j.materresbull.2018.11.030

[17]. N.-L. Liu, S.-H. Sun, C.-H. Hou, *Sep. Purif. Technol.* 215 (2019) 403–409. DOI: 10.1016/j.seppur.2019.01.029

[18]. G. Zhu, H. Wang, H. Xu, L. Zhang, *J. Electroanal. Chem.* 822 (2018) 81–88. DOI: 10.1016/j.jelechem.2018.05.024

[19]. D.K. Kohli, R. Singh, M.K. Singh, A. Singh, R.K. Khardekar, P. Ram Sankar, P. Tiwari, P.K. Gupta, *Desalin. Water Treat.* 49 (2012) 130–135. DOI: 10.1080/19443994.2012.708210

[20]. V. Pavlenko, Q. Abbas, P. Przygocki, T. Kon'kova, Zh. Supiyeva, N. Abeykoon, N. Prikhodko, M. Bijsenbayev, A. Kurbatov, B.T. Lesbayev, Z. Mansurov, *Eurasian Chem.-Technol. J.* 20 (2018) 99–105. DOI: 10.18321/ectj695

[21]. S. Azat, R. Busquets, V. Pavlenko, A. Kerimkulova, R. Whitby, Z. Mansurov, Applied Mechanics and Materials 467 (2014) 49–51. DOI: 10.4028/www.scientific.net/AMM.467.49

[22]. J. Jagiello, J.P. Olivier, *Carbon* 55 (2013) 70–80. DOI: 10.1016/j.carbon.2012.12.011

[23]. F. Stoeckli, M.V. López-Ramón, D. Hugi-Cleary, A. Guillot, *Carbon* 39 (2001) 1115–1116. DOI: 10.1016/S0008-6223(01)00054-9

[24]. Z.R. Ismagilov, N.V. Shikina, I.P. Andrievskaya, N.A. Rudina, Z.A. Mansurov, M.M. Burkitbaev, M.A. Biisenbaev, A.A. Kurmanbekov, *Catal. Today* 147 (2009) 58–65. DOI: 10.1016/j.cattod.2009.07.043